Statistics of Storm Updraft Velocities from TWP-ICE Including Verification with Profiling Measurements

SCOTT COLLIS

Environmental Science Division, Argonne National Laboratory, Argonne, Illinois

ALAIN PROTAT AND PETER T. MAY

Centre for Australian Weather and Climate Research, Australian Bureau of Meteorology, Melbourne, Australia

CHRISTOPHER WILLIAMS

Cooperative Institute for Research in Environmental Sciences, University of Colorado Boulder, and NOAA/Earth System Research Laboratory, Boulder, Colorado

(Manuscript received 22 August 2012, in final form 8 March 2013)

ABSTRACT

Comparisons between direct measurements and modeled values of vertical air motions in precipitating systems are complicated by differences in temporal and spatial scales. On one hand, vertically profiling radars more directly measure the vertical air motion but do not adequately capture full storm dynamics. On the other hand, vertical air motions retrieved from two or more scanning Doppler radars capture the full storm dynamics but require model constraints that may not capture all updraft features because of inadequate sampling, resolution, numerical constraints, and the fact that the storm is evolving as it is scanned by the radars. To investigate the veracity of radar-based retrievals, which can be used to verify numerically modeled vertical air motions, this article presents several case studies from storm events around Darwin, Northern Territory, Australia, in which measurements from a dual-frequency radar profiler system and volumetric radar-based wind retrievals are compared. While a direct comparison was not possible because of instrumentation location, an indirect comparison shows promising results, with volume retrievals comparing well to those obtained from the profiling system. This prompted a statistical analysis of an extended period of an active monsoon period during the Tropical Warm Pool International Cloud Experiment (TWP-ICE). Results show less vigorous deep convective cores with maximum updraft velocities occurring at lower heights than some cloud-resolving modeling studies suggest.

1. Introduction

The regionalization of global climate models has been a driver of demand for more complex convective parameterization schemes. A key readjustment of the modeled atmosphere involves the mass flux over the grid cell, which is linked to vertical motions in storm systems. The vertical component of storm dynamics has a large impact on the life cycle of convective systems. While use of large-scale measurements to validate cloud-resolving models has been attempted (e.g., Varble et al. 2011), a thorough evaluation of in-cloud vertical air motions produced by numerical models at different scales of motion (from high-resolution cloud-resolving to climate models) is still pending. While works such as Yuter and Houze (1995b) produce statistical views of individual events, a longer sampling period is required to account for the natural storm-to-storm variability, which cannot be captured in cloud-resolving models. Two major recent efforts to validate climate model vertical air motions have even used cloud-resolving model vertical air motions instead of observations (Wang and Liu 2009; Wu et al. 2009). In situ measurement of vertical velocities is relatively straightforward with aircraft probes, but is not directly comparable with climate model outputs because of the vast difference in temporal and spatial scales.

Corresponding author address: Scott Collis, Environmental Sciences Division, Argonne National Laboratory, Building 240, 9700 South Cass Ave., Argonne, IL 60439.
E-mail: scollis@anl.gov

DOI: 10.1175/JAMC-D-12-0230.1

Two potential measurement types may bridge this observational gap between in situ observations and climate models: vertically pointing (soda straw) measurements that sample a fixed (in space) vertical column, such as those produced by wind profilers, and full three-dimensional volumetric measurements, such as those produced by scanning Doppler radars, for example as reported for Florida in Yuter and Houze (1995a). The ultimate goal is to have a complete chain of comparisons including point measurements, vertically pointing measurements, and volumetric measurements followed by comparisons with modeled quantities using a hierarchy of models. Both profiling and volumetric measurements have different advantages and shortcomings. Profilers at frequencies around 50 MHz have been used to directly measure vertical motions in convection, but only for a given vertical column (e.g., Cifelli and Rutledge 1994; May and Rajopadhyaya 1996, 1999; May et al. 2002). Retrievals from scanning Doppler weather radars (e.g., Ray et al. 1980; Gamache et al. 1995) allow for unique insights into storm dynamics at the mesoscale, including vertical air motions, but the vertical air motions are retrieved in a more indirect way, using the airmass continuity equation and Doppler radar measurements.

The work presented in this paper uses observations near Darwin, Northern Territory, Australia, collected during the Tropical Warm Pool International Cloud Experiment (TWP-ICE) (May et al. 2008). The Darwin area hosts an extensive ground-based observational network that includes Australian Bureau of Meteorology scanning Doppler radars and radar wind profilers as well as the U.S. Department of Energy Atmospheric Radiation Measurement Program (ARM) Climate Research Facility (ACRF) site (Ackerman and Stokes 2003).

This paper compares retrievals from the profiling and volumetric techniques in an effort to qualitatively verify the vertical velocities retrieved from the volumetric data and is complementary to work described in Reasor et al. (2009), which highlighted detailed efforts in validating airborne Doppler wind retrievals with in situ measurements. The methods used to retrieve vertical air motions from dual-frequency profiler techniques and scanning Doppler weather radar observations are described in section 2. Case studies typical of convective organization around Darwin are then analyzed, and vertical air motion retrievals are compared in section 3. Section 4 describes the statistical properties of vertical air motion as derived for the active phase of a monsoon, which can be readily compared with the model study of Wu et al. (2009). Conclusions are presented in section 5.

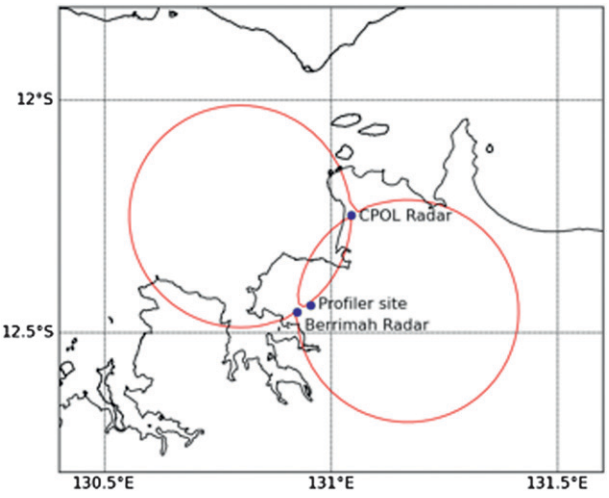

FIG. 1. Layout of the profiling and scanning radar systems around Darwin during the TWP-ICE field program. The red lines denote where the angles of intersection between the radar beams (from the Berrimah and CPOL radars) are 150° or 30°. These are known as the dual-Doppler lobes and represent areas of increased confidence in the retrieved winds.

2. Retrieving vertical air motions within precipitation

There are three techniques for measuring vertical motions in precipitation. First is direct measurement with in situ aircraft probes, which are accurate but undersample the strong updraft cores because of the danger of aircraft penetrating high-reflectivity cores where hail and strong vertical velocities may be present. Second, profiling radars operating at 50 MHz are predominantly sensitive to Bragg scattering of turbulent structures assumed to be ''frozen in'' the upward- and downward-moving air parcels. One limitation of profiling radars is that they only sample the cloud systems that pass directly over the profiler site. The third technique uses two scanning Doppler weather radars to measure hydrometeor motion throughout a large volume and retrieve the three-dimensional wind motion through the volume of precipitation. This third technique is a less direct measurement than either an in situ or vertically pointing measurement, but it captures mesoscale storm motions allowing for direct comparisons with modeling output, given the same resolved scales. The next two subsections describe vertical air motions retrieved from dual-frequency profiling radars and from two scanning Doppler weather radars.

a. Dual-frequency wind profiler retrievals

A 50-MHz profiler radar located about 8 km southeast of the ACRF site (as shown in Fig. 1), hereinafter also called a very high-frequency (VHF) profiler, can simultaneously

observe vertical air motion due to Bragg scattering from turbulent inhomogeneities in refractive index (Balsley and Gage 1982; Gage et al. 1994) and hydrometeors due to Rayleigh scattering (Fukao et al. 1985; Wakasugi et al. 1986). The Bragg and Rayleigh scattering processes will appear in two regions of the 50-MHz profiler Doppler velocity spectra with the Rayleigh scattering always moving downward relative to the Bragg scattering. The collocated 920-MHz profiler (hereinafter also called UHF profiler) cannot observe vertical air motion during precipitation, but it can observe hydrometeors due to Rayleigh scattering (Carter et al. 1995).

A new dual-frequency vertical air motion retrieval technique uses 920-MHz profiler observations to mask the hydrometeor signal in the 50-MHz profiler Doppler velocity power spectra before identifying the vertical air motion signal (Williams 2012). The dual-frequency technique calculates the first three moments of the Bragg scattering signal: signal-to-noise ratio (SNR), mean radial velocity (air motion minus hydrometeor motion), and spectrum width. When no hydrometeors are observed by the 920-MHz profiler, no dual-frequency hydrometeor masking is needed before estimating the three moments of the vertical air motion. Monte Carlo simulations of simulated 50-MHz profiler spectra show that Bragg scattering spectra are symmetrical so that the vertical air motion retrieval uncertainties are independent of vertical velocity, but dependent on SNR and spectrum width. Observed SNR and spectrum width values from the Darwin 50-MHz profiler during TWP-ICE (Williams 2012) suggest retrieval uncertainties rarely exceed $0.5\,\mathrm{m\,s^{-1}}$ (see Fig. 3 in section 3a). Illustrations of dual-frequency vertical air motions within stratiform clouds are given in Protat and Williams (2011).

b. *Multipass variational wind retrieval from scanning Doppler weather radar observations*

In the cases investigated in this study, data were collected from the operational Bureau of Meteorology Doppler radar at Berrimah, a suburb of Darwin, and the C-band polarimetric (CPOL; Keenan et al. 1998) research radar at Gunn Point (Fig. 1). The scan strategies of both radars were configured to perform dual-Doppler velocity analysis with coordinated volume scans collected every 10 min. Volume scans required 8 min to collect all plan position indicator (PPI) scans, and both radars were synchronized and used scanning modes designed to fully sample the vertical extent of the precipitating systems. With Nyquist velocities of the Berrimah and CPOL radars set to 8.9 and $13.8\,\mathrm{m\,s^{-1}}$, respectively, it was essential to dealias the radial Doppler velocities. We used the four-dimensional dealiasing method of James and Houze (2001). While this technique worked well most of the time, because of the low Nyquist occasional folds were missed (picked up during visual inspection), requiring a perturbation of the first-guess field in order to retrieve a dealiased field. In the second radar processing step, dealiased radial velocities were interpolated onto a common Cartesian coordinate grid using a mixed-order linear interpolation algorithm (to suppress gridding artifacts where the sampling is poor; see Collis et al. 2010). Each gridded cell contained a reflectivity and radial Doppler velocity from both scanning radars at a 1 km × 1 km horizontal and 500-m vertical resolution. Both radars fully covered the domain shown in Fig. 1. The temporal resolution was set by the synchronized volume scan sequence of 10 min. Third, surface clutter signals were identified to generate a data rejection mask that was applied to all gridded volumes and influenced only the lowest gridded heights.

In the fourth and final processing step, the three-dimensional motions were retrieved from the gridded radial velocities using a technique first reported in Ray et al. (1980) and further developed in Scialom and Lemaître (1990) and Protat and Zawadzki (2000), among many others. The technique involves the minimization of a cost function:

$$J = J_m + J_c + J_s, \tag{1}$$

using a conjugate gradient minimization algorithm. The three terms J_m, J_s, and J_c are the costs due to radial velocity measurement disparity, noise in the retrieval, and anelastic continuity equation disparity, respectively. The radial velocity measurement disparity is given by

$$J_m = \frac{1}{2}\sum(v_r' - v_r)^2 = \frac{1}{2}\sum\{[c_x u + c_y v + c_z(w - w_t)] - v_r\}^2, \tag{2}$$

where v_r is the radial projection of the current guess for the velocity components with v_r' denoting the current guess; u and $w - w_t$, v_r are the gridded measured radial velocities (in the meridional, zonal, and vertical directions where w_t is the hydrometeor fall speed); and c_x, c_y, and c_z are the unit vectors for the propagation of the beam and the sum is over all grid points and radars. The fall speed of the scattering hydrometeors w_t is calculated from a simple empirical reflectivity fall speed relation given in (Caya 2001). The fall speed relation is one area of the retrieval that can be optimized (for example including polarimetric information) but is left for future work.

The term J_s, designed to remove rapid variations in the retrieval, is also known as the smoothness constraint and is given by

$$J_s = a[F(u) + F(v)], \quad \text{with} \tag{3}$$

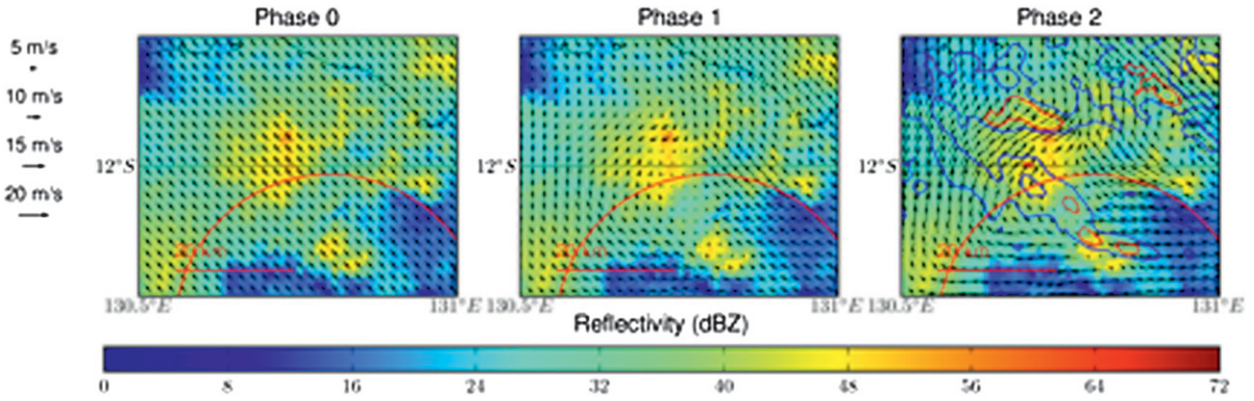

FIG. 2. Overhead views of the retrieved wind field (vectors) overlaid on the CPOL-derived reflectivity (color mesh background) at 4000-m height. Contours depict vertical velocities of 2 (blue), 4 (red), and 8 (yellow) $m\,s^{-1}$. The red ring is the outer edge of the dual-Doppler lobes and data to the north and northwest are outside the traditional dual-Doppler coverage. Data are taken from 19 Jan 2006 during TWP-ICE. (left) Phase 0 shows the sounding first guess, (center) phase 1 shows the retrieval with a higher smoothing weight, and (right) phase 2 shows the final retrieval with the continuity constraint introduced to allow the retrieval of vertical motions.

$$F(\psi) = \left(\frac{\partial^2\psi}{\partial x^2}\Delta x^2\right)^2 + \left(\frac{\partial^2\psi}{\partial y^2}\Delta y^2\right)^2 + \left(\frac{\partial^2\psi}{\partial z^2}\Delta z^2\right)^2 + 2\left(\frac{\partial^2\psi}{\partial x\partial y}\Delta x\Delta y\right)^2 + 2\left(\frac{\partial^2\psi}{\partial x\partial z}\Delta x\Delta z\right)^2 + 2\left(\frac{\partial^2\psi}{\partial y\partial z}\Delta y\Delta z\right)^2, \quad (4)$$

where Δx, Δy, and Δz are the grid spacing in the meridional, zonal, and vertical directions, respectively. The weighting constant a controls the strength of the smoothing constraint and is chosen to suppress noise and similar artifacts but not to suppress convergent and divergent structures. Sensitivity studies have suggested a value of 0.05 allowed for good noise suppression without filtering out the retrieval resolution too much.

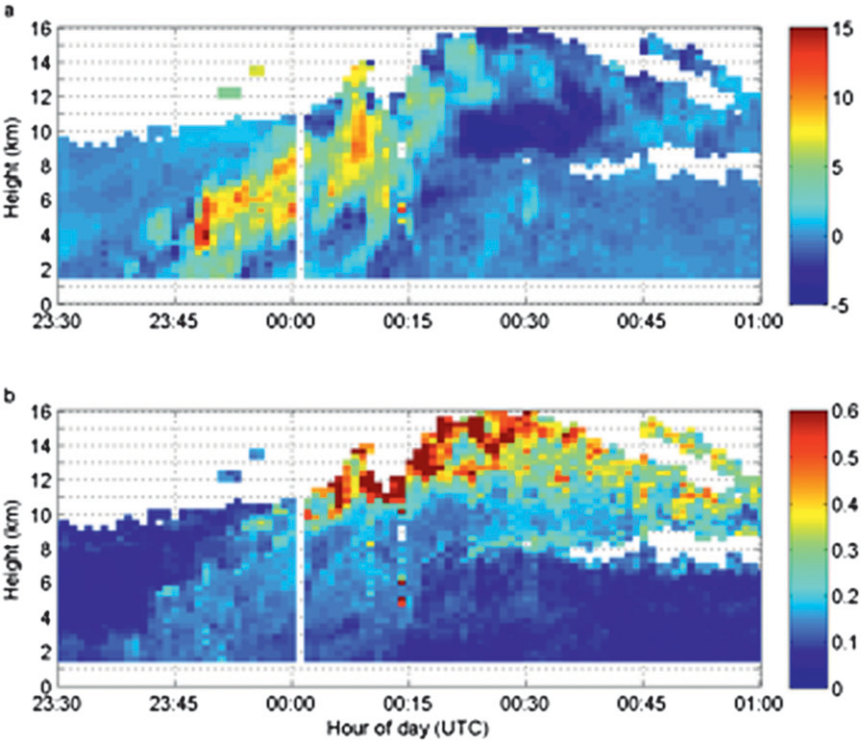

FIG. 3. Vertical air motions retrieved from the dual-frequency (50/920 MHz) profiler system for (a) a squall line case and (b) estimated retrieval uncertainty.

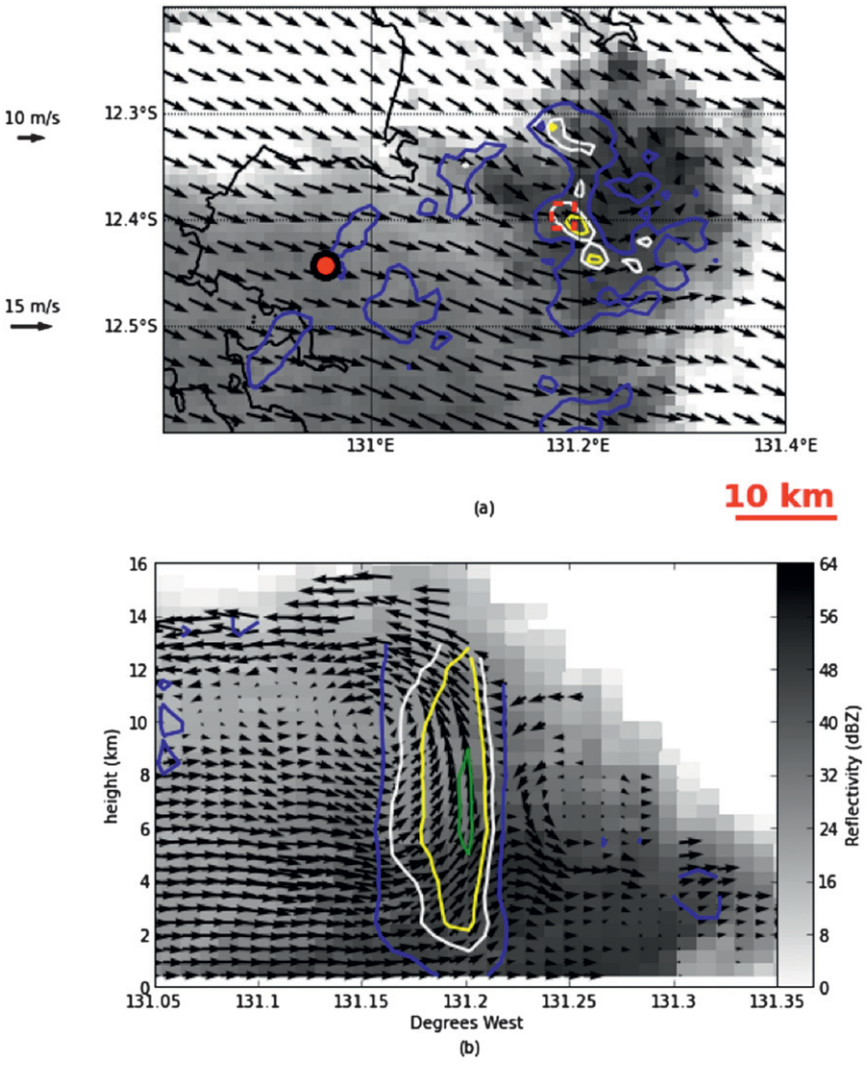

FIG. 4. Retrieved wind motions from dual-Doppler-derived radial velocities for an eastward-propagating squall line at 1150 UTC 19 Jan 2006. (a) Constant-height (3500 m) slice through the data showing the mapped reflectivity field (as seen by the CPOL radar) and vectors representing the meridional and zonal components of the radar-derived wind field. The red box shows the storm feature that passed over the profiler (depicted as a red dot) site 60 min earlier (assuming the feature moved at the storm motion vector). (b) A constant latitude slice through the data at 12.4°S with the vectors showing the zonal and vertical components of the derived wind field. In both plots, the contours depict lines of constant vertical velocity with blue, white, yellow, and green being 1, 4, 6, and 10 m s^{-1}, respectively.

The final constraint in the cost function allows the retrieval of the vertical motions. The term J_c is the air-mass continuity equation constraint using the vertical weighting scheme proposed in Protat and Zawadzki (1999) and is expressed as

$$J_c = \frac{1}{2}\sum\left[w' - \left(\frac{z_{\text{top}} - z}{z_{\text{top}}} w_c\uparrow + \frac{z}{z_{\text{top}}} w_c\downarrow\right)\right]^2, \quad (5)$$

where w' is the current guess for the vertical velocity, z is the height, z_{top} is the height of the top of the integration, and $w_c\uparrow$ and $w_c\downarrow$ are the vertical velocities obtained from an upward and downward integration of the anelastic mass continuity equation

$$\frac{1}{\rho}\frac{\partial w_c \rho}{\partial z} = -\nabla v_h, \quad (6)$$

where ρ is the atmospheric density and v_h is the horizontal wind flow (u, v). The choice of boundary conditions used for the vertical integrals is a potential source of error. Using $w_c\uparrow = 0$ at $z = 0$ and $w_c\downarrow = 0$ at $z = z_{\text{top}}$ is

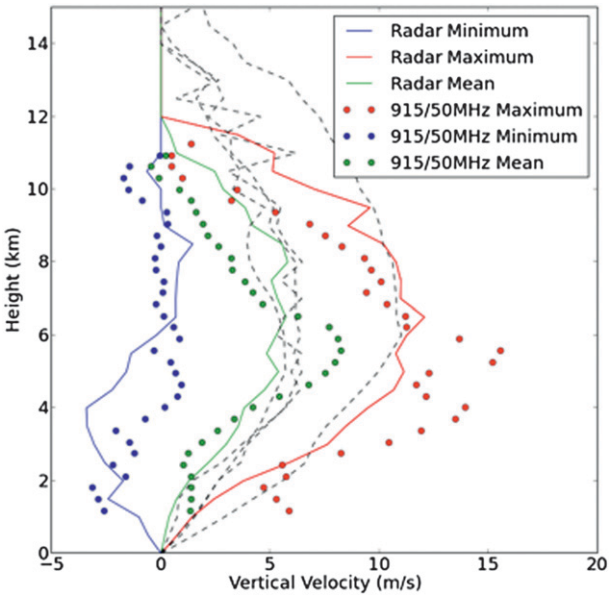

FIG. 5. Vertical velocities retrieved from dual profiler (50/920 MHz) measurements (circles) and from an equivalent advected column of radar-derived radial velocities (lines). Blue shows the minimum vertical velocity in the time period and sample volume, red depicts the maximum vertical velocity, and green shows the mean vertical velocities. The dashed lines show the maximum vertical velocity for dual-Doppler time steps before and after the "ideal" time step when the system propagated into the dual-Doppler domain. This comparison is for the case depicted in Fig. 4.

a natural choice. However, given that the lowest elevation of the radar volume is above zero (0.5° for the CPOL and Berrimah radars), the height at which vertical velocities will become nonzero may not be captured in the radar scans. Studies using combined wind profiler and radio acoustic sounding system measurements (May 1999) show vertical velocities up to $2\,\mathrm{m\,s^{-1}}$ at 217 m above the ground. To compensate for this issue, we have implemented a subradar convergence–divergence infill algorithm. During the vertical integration stage, the algorithm checks to see if there is a valid return at a height corresponding to the lowest elevation of the radar at that range. If a valid return is detected, the column is tagged as a "cloud on ground" column. For cloud-on-ground columns, the convergence or divergence from $z = 0$ to the height of the cloud-on-ground grid cell is set to the same as the cloud-on-ground grid cell. The subcoverage convergence or divergence is then used in the upward and downward integral in addition to the calculated convergences or divergences at other levels. The impact of this on the final retrieved vertical velocity varies as a function of storm morphology. (However, from a statistical sense, the impact on convective cores presented in Fig. 11, described in section 4, is to raise the 99th-percentile updraft by $\sim 2\,\mathrm{m\,s^{-1}}$.)

At the start of the retrieval process the initial cost is calculated using a first-guess field. The present study uses a three-phase system. The first phase is simply derived from soundings (but could also be derived from model or reanalysis); this is used as first guess for the second phase, a retrieval of the horizontal winds ($J_c = 0$) with strong smoothing of $a = 0$. The slowly varying horizontal wind retrievals are then used to initialize the full three-dimensional wind field retrieval (phase three) with $a = 0.05$. Figure 2 shows the three phases of retrieval with sounding-derived winds on the left, first-pass winds in the center, and full retrieval (with updrafts contoured) on the right. By first retrieving the broad-scale flow, the cost function is closer to the true minima, rather than the local minima, when the full retrieval is performed.

Because of the variational nature of the retrieval algorithm, uncertainty characterization is nontrivial. Sources of uncertainty include noise in the data; the smearing out of convergent and divergent structures due to the beamwidth and undersampling of structures aloft because of a sparser scanning pattern; errors due to the simplicity of the fall speed correction (although this is secondary, as it only impacts the comparison to the radial velocity in determining the measurement cost); and, finally, the impact of radial velocity artifacts, which, as discussed in Collis et al. (2010), are generated by using linear techniques to grid sparsely sampled nonlinear phenomena (a classic example is "waves" in mapped brightband melting-layer signatures in mapped reflectivity data) and can be on the order of $1\,\mathrm{m\,s^{-1}}$. A detailed analysis is not presented in this paper but is the subject of an ongoing sensitivity study based at the ARM Southern Great Plains site where many more profiling systems exist.

3. Verification of variationally retrieved vertical velocities from scanning Doppler radars

The previous section (2b) outlined the methodology for retrieving storm motions, including vertical velocities, from scanning Doppler radar-derived radial velocities. Given the assumptions made and issues having to do with adequate resolving of convergent and divergent features and with radar coverage, what is the accuracy of volumetric dual-Doppler retrievals over Darwin, both in terms of confidence intervals and bias? To validate the procedure, vertical velocities using the techniques outlined in section 2a will be compared with those retrieved from two scanning Doppler radars (CPOL and the operational Berrimah radar) in Darwin.

Figure 1 shows the layout of instrumentation around Darwin. The profiler site is approximately 3.5 km

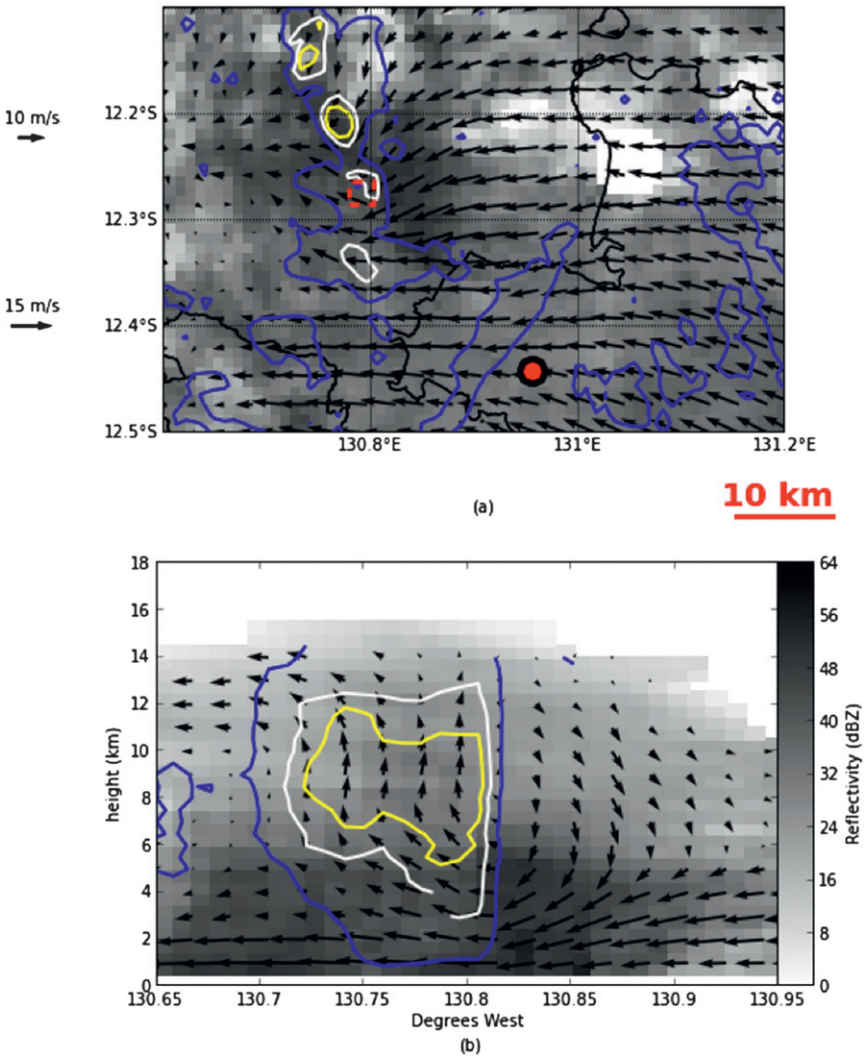

FIG. 6. As in Fig. 4, but for an embedded convective core in a stratiform region sampled on 18 Feb 2006 with the constant latitude slice being at 12.27°S.

west-northwest from the Berrimah radar, and roughly along the baseline between the Berrimah and CPOL radars, where the multi-Doppler technique cannot be used with confidence for vertical air motion retrievals because of the profiler's proximity to the Berrimah radar [most of the precipitating systems are not topped by the highest (47°) radar elevation angle]. This prevents a direct comparison between profiler-derived and scanning Doppler radar-derived winds.

To use the profiler vertical velocity measurements, an indirect comparison was performed. The profiler observations were examined for events of interest, and the volumetric observations were used to narrow this set down to a series of events such that the system of interest propagated over the profiler and into a region conducive to multi-Doppler wind retrieval. By observing the feature at different time steps, an advection speed and direction were derived allowing the feature that had passed over the profiler site. This feature was then isolated from the rest of the retrieved winds and the minimum (downdraft), mean, and maximum (updraft) vertical velocities were calculated. The same procedure of extracting the minimum, mean, and maximum vertical velocity for the feature was performed on the dual-frequency profiler-derived vertical velocities. This methodology has the advantage of comparing vertical air motions measured within the same convective elements, the drawback being that they are not measured at exactly the same time, but with a time difference that depends on the propagation speed of the cell under consideration. Systems were propagating fast enough that only a few scans (~20 min) passed. It should be noted that this study aims to determine

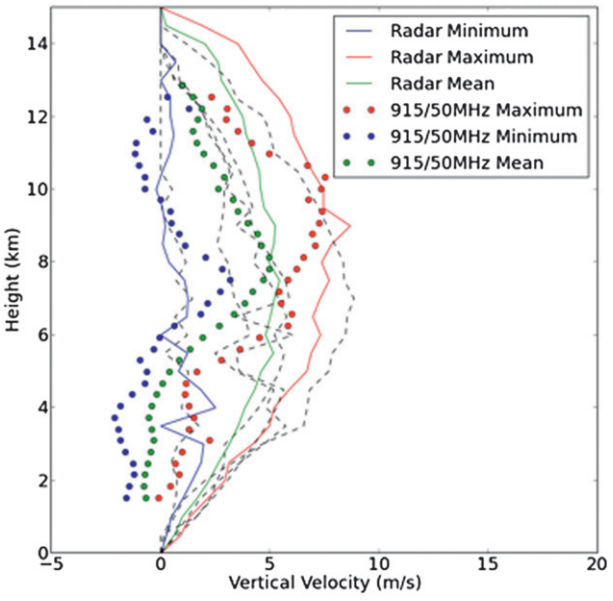

FIG. 7. As in Fig. 5, but for the case depicted in Fig. 6.

the qualitative accuracy of the multi-Doppler retrievals. In the current instrument configuration, a one-to-one comparison is not possible.

Three cases were chosen to verify the multi-Doppler retrievals, as they correspond to different types of precipitating systems with different expected vertical velocity magnitudes and profiles. Cases are drawn from the TWP-ICE (May et al. 2008) intensive observation period (IOP) and a short period following the IOP (from 19 January to 14 February) during the 2006 wet season in Darwin.

a. Squall line

A squall line was observed on 19–20 January 2006 when an active monsoon trough was present over the Darwin area. During this period, a series of squall lines propagated over the Darwin area with the resulting outflow generating stratiform precipitation in its wake. The leading edge of such an event passed over the profiler site at around 2350 UTC 19 January 2010. The dual-frequency retrieval vertical air motions are shown in Fig. 3a with updrafts exceeding $10\,m\,s^{-1}$. The estimated vertical air motion uncertainties are shown in Fig. 3b and show that uncertainties exceed $0.5\,m\,s^{-1}$ near the edge of the profiler's detectable range, varying from 10–12 to 14–16 km. This is primarily due to decreasing SNR. Note that the retrieval uncertainties are approximately $0.2\,m\,s^{-1}$ from 4 to 10 km in the updraft core. The storm then propagated east-northeast into a region conducive to multi-Doppler analysis. Figure 4 shows overhead (Fig. 4a) and constant longitude (Fig. 4b) slices through the retrieved winds (vectors). The vectors were thinned down from 1 km to a resolution of 2 km. The figure shows an updraft complex upwind of the reflectivity maximum. Figure 4b shows elevated echo tops coincident with the $\sim 10\,m\,s^{-1}$ updraft. The red line in Fig. 5 shows the maximum updrafts as a function of height across the feature, the green line shows the mean values, and the blue line shows the maximum (magnitude) downdrafts. The red, green, and blue circles show the same quantities but from the profiler across an equivalent temporal extent (determined using the advection speed, approximately 20 min of profiler data for a 3 km × 3 km box in the dual-Doppler data). The black dashed lines show maximum vertical velocities from other, less ideal, time steps and give an idea of the temporal evolution and uncertainty. Given the differing scales and the evolution of the feature as it advected the comparison is very close. The profiles above 4.5 km only differ by around $1\,m\,s^{-1}$ at most heights. The agreement is not as good below, but again this could either be due to time lag between observations (again, as highlighted by the dashed black lines) or a deficiency in the multi-Doppler or dual-frequency retrieval. Comparing with Table 2 of Reasor et al. (2009), where over the period of their study the authors see a bias of $0.31\,m\,s^{-1}$ and an RMSE of $1.50\,m\,s^{-1}$ (in situ vs retrieval), it is more likely that it is the evolution of the system causing the disparity. While, ideally, we would like to reproduce the statistics of the aforementioned study, the experimental setup does not allow for direct comparison, although in section 3d we do a more quantitative analysis over multiple cases. Still, this first case study gives good confidence that, despite the coarse sampling of a plan position indicator volumetric scan, convergent structures were well enough resolved [using Eq. (6)] to reproduce a reasonable measurement of vertical velocity.

b. Embedded convective system

A monsoon trough to the north of Darwin and a weak low to the southeast of Darwin generated widespread rainfall with embedded convective cells throughout the Darwin area. Figure 6 shows retrieved winds for 1500 UTC 18 February 2006. The overhead view (Fig. 6a) shows an embedded squall feature with reflectivity maxima behind the updraft structure. The elevated echo tops are consistent with retrieved updraft locations. Comparisons between maximum updrafts and downdrafts in Fig. 7 show that the multi-Doppler vertical air motions are in broad agreement on the shape of the profile with the dual-frequency profiler vertical air motions at higher elevations. The overall magnitude of vertical velocities retrieved from multi-Doppler is less (a negative bias of $\sim 2.5\,m\,s^{-1}$), which could be due to

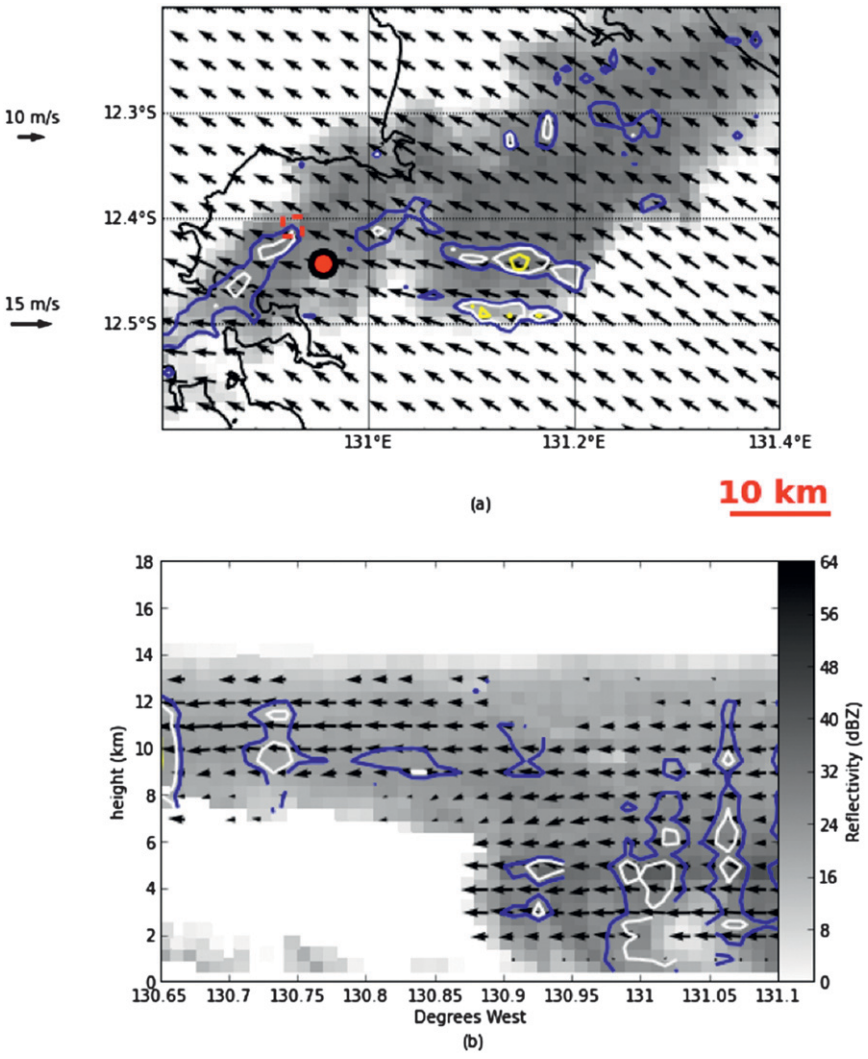

FIG. 8. As in Fig. 4, but for a thick precipitating cirrus layer (anvil remnant) with the constant latitude slice at 12.41°S and the blue, white, yellow, and green contours are equal to 0.5, 1, 2 and 3 m s^{-1}.

the system evolving as it propagated from a continental environment into the warm waters of Darwin harbor or, again, deficiencies in either technique.

c. *Anvil cirrus detrained from convection*

On 10 February 2006, a squall line passed to the south of Darwin with very thick cirrus outflow advecting over the profiler site. Occasional precipitation was observed over the profiler site but there was no large updraft activity. Figure 8 shows the retrieved winds at 1320 UTC. The interest of using such a case study is that presumably vertical air motions are weaker than in the two previous case studies, thereby evaluating the capacity of the multi-Doppler technique to retrieve weak vertical air motions. This is confirmed in Fig. 8 with absolute vertical air motions not exceeding 2 m s^{-1}. The comparison between the two retrievals (Fig. 9) shows that, in this weak vertical air motion case, the multi-Doppler technique is able to reproduce the magnitude of the maximum updraft and downdraft profiles as retrieved from the dual-frequency technique. Differences observed are again less than ~0.5–1 m s^{-1} at most heights. The features are not correlated, although this is unsurprising given the weak forcing.

d. *Cross-case comparison*

All the data from the cases studied previously were concatenated, and the profiler-retrieved vertical velocities were interpolated onto the multi-Doppler vertical levels. Figure 10 shows a plot of profiler-derived vertical

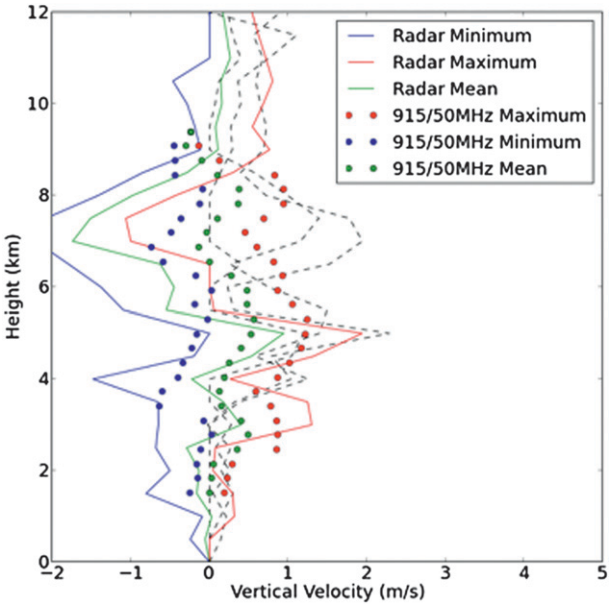

FIG. 9. As in Fig. 5, but for the case depicted in Fig. 8.

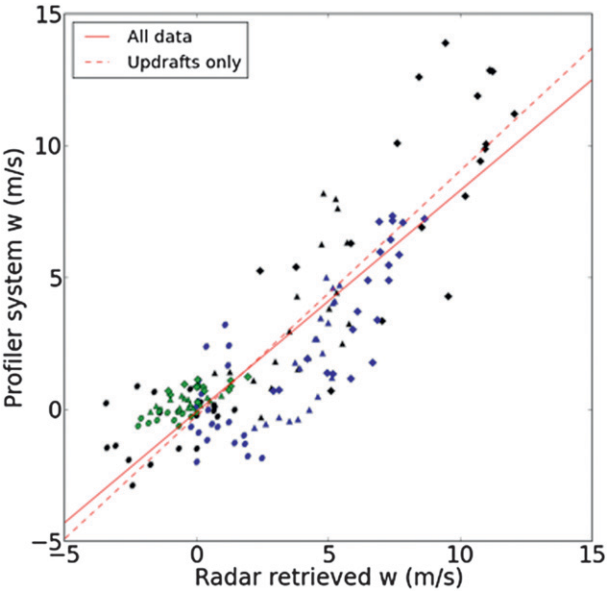

FIG. 10. A scatterplot of profiler-derived vertical velocities vs the scanning radar-retrieved vertical velocities. Dots represent minimum, triangles mean, and diamonds maximum values. The solid line is a fit to all maximum, mean, and minimum values while the dashed line is a fit to maximum values only. The different colors represent the different cases presented in the study with the squall in black, the embedded system in blue, and the cirrus case in green.

velocities versus those derived from the radar-measured radial velocities using the variational technique. Diamonds represent the maximum values, triangles represent mean values, and dots represent the minimum values. Linear fits were performed on the whole dataset (solid line) and the maximum values only (dashed line). The solid line has a gradient of 0.83 m s^{-1} and the RMS difference between the line and data is 1.9 m s^{-1}. The dashed line has a gradient of 0.93 m s^{-1} and an RMS difference of 2.2 m s^{-1}. The data are strongly correlated, with correlation coefficients of 0.85 and 0.84, respectively. The results presented in this study show that the updrafts retrieved using the variational technique have a very slight negative bias but less than the data spread. Comparing, again, with Table 2 of Reasor et al. (2009), and noting that the authors of that study performed a direct comparison with in situ data, the RMSE is comparable but the (negative) bias is larger. Given the possible issues with the advection technique required because of the profiler location, this shows that the variational retrieval technique is returning values where the bias is within the variability of the values as compared with the profiler measurements.

4. Statistical updraft properties for the wet monsoon period of TWP-ICE

Because of the stochastic nature of precipitating systems, cloud-resolving models cannot be expected to reproduce the same vertical velocity morphology as observed with remote sensing systems for individual storms. Having established that the variational retrieval technique is able to retrieve reasonable vertical air motions, it is possible to build a statistical picture of vertical motions in precipitation around Darwin by performing retrievals over a statistically significant time frame. A subset of the TWP-ICE model intercomparison period (Fridlind et al. 2012) was chosen that aligned with the period modeled using Weather Research and Forecasting (WRF) and the National Aeronautics and Space Administration Goddard Institute for Space Studies GCM as reported in Wu et al. (2009). This period, hereinafter known as the wet monsoon, is from 0400 UTC 19 January to 0000 UTC 22 January 2006. This was an active phase of the monsoon in which the monsoon trough dipped toward Darwin, drawing moist, latently unstable air over the region. Figure 11 shows the statistical coverage product (May and Lane 2009), which is the percentage of the area in the rectangular domain containing the dual-Doppler lobes (Fig. 1; 145 km × 125 km centered on CPOL) covered by reflectivity above a particular threshold. The figure shows extensive coverage peaking particularly in the local early morning (around 1800–2200 UTC). As shown in Fig. 11b, the stronger returns are confined to below the freezing level (evident as a brightband signal at ~5 km). This is in contrast to break

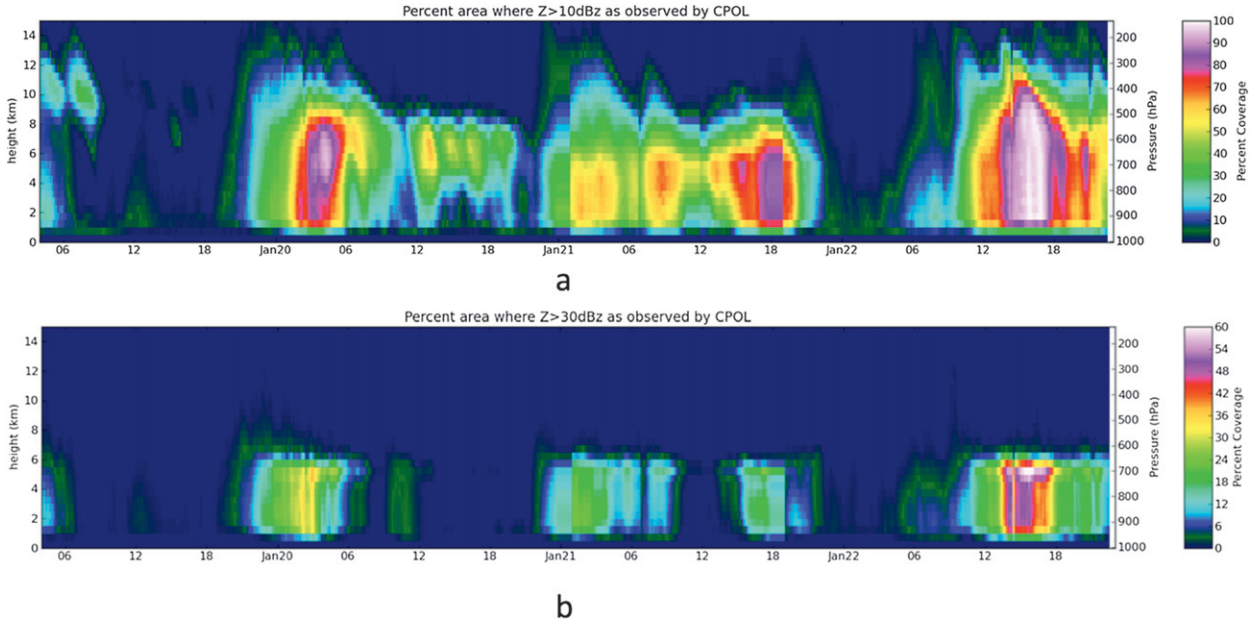

FIG. 11. The percentage of the mapped radar domain ($145 \times 125\,\text{km}^2$ centered on CPOL) containing returns greater than (a) 10 and (b) 30 dBZ. This statistical coverage product shows the domain-wide evolution of the precipitating system during the wet monsoon period of TWP-ICE from 19 Jan to 0000 UTC 22 Jan 2006.

storms, such as Hector, for which there are extensive regions of high reflectivity above the freezing level due to large hail lofted by strong updrafts (May and Lane 2009). The data from the Berrimah and CPOL radars were collected (522 individual time steps), dealiased, quality controlled (visually inspected), and mapped onto a Cartesian grid. The variational algorithm described in section 2b was then used to retrieve three-dimensional three-component wind vectors. To compile similar statistics to the modeling studies, we defined a deep convective column (DCC) in the dual-Doppler dataset to be a column of data in which there are vertical velocities equal to or exceeding $1\,\text{m s}^{-1}$ for at least 5 km in height. This varies slightly from the conditional sampling in Wu et al. (2009), as it does not include a hydrometeor content requirement (of a hydrometeor mixing ratio $r_h \geq 10^{-4}\,\text{kg kg}^{-1}$). However, since these retrievals were constrained to regions where the CPOL returns were greater than 1 dBZ, it can be assumed that this constraint was met.

Two datasets were compiled from the retrievals: all vertical motions within the dual-Doppler lobes (Fig. 1) and all vertical motions within the dual-Doppler lobes that are also in a DCC. Note that the second dataset contains all points in DCCs including those below the $1\,\text{m s}^{-1}$ threshold, including downdrafts. All values of vertical velocity at a particular height were collated, and for each level the values of the 99th, 95th, and 50th percentiles as well as the mean were calculated; these are plotted in Fig. 12 as a function of height. The left-hand side shows the complete dataset within the dual-Doppler lobes, while the right-hand side shows the conditional percentiles in DCCs as a function of height.

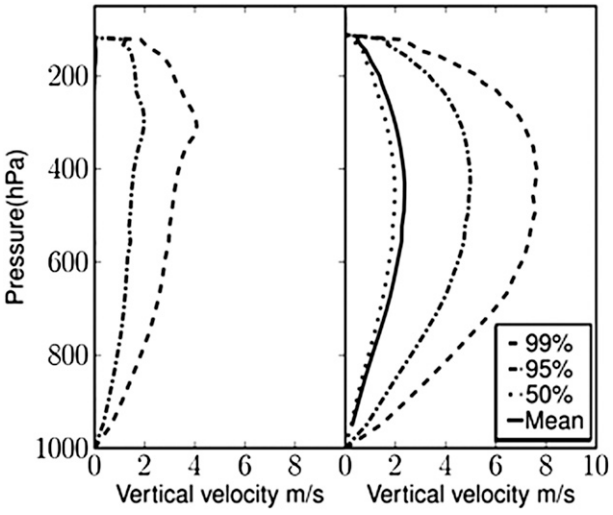

FIG. 12. Plots of the 99th, 95th, and 50th percentiles and the mean vertical velocities retrieved over the wet monsoon period of TWP-ICE (from 0400 UTC 19 Jan to 2350 UTC 22 Jan 2006, as depicted in Fig. 10). The left-hand side corresponds to all valid returns in the dual-Doppler lobes (Fig. 1) while the right-hand side is a conditional sample for columns that have at $w > 1\,\text{m s}^{-1}$ for at least 5 km of depth. The left-hand side isolates deep convective cores to allow comparison with Fig. 13.

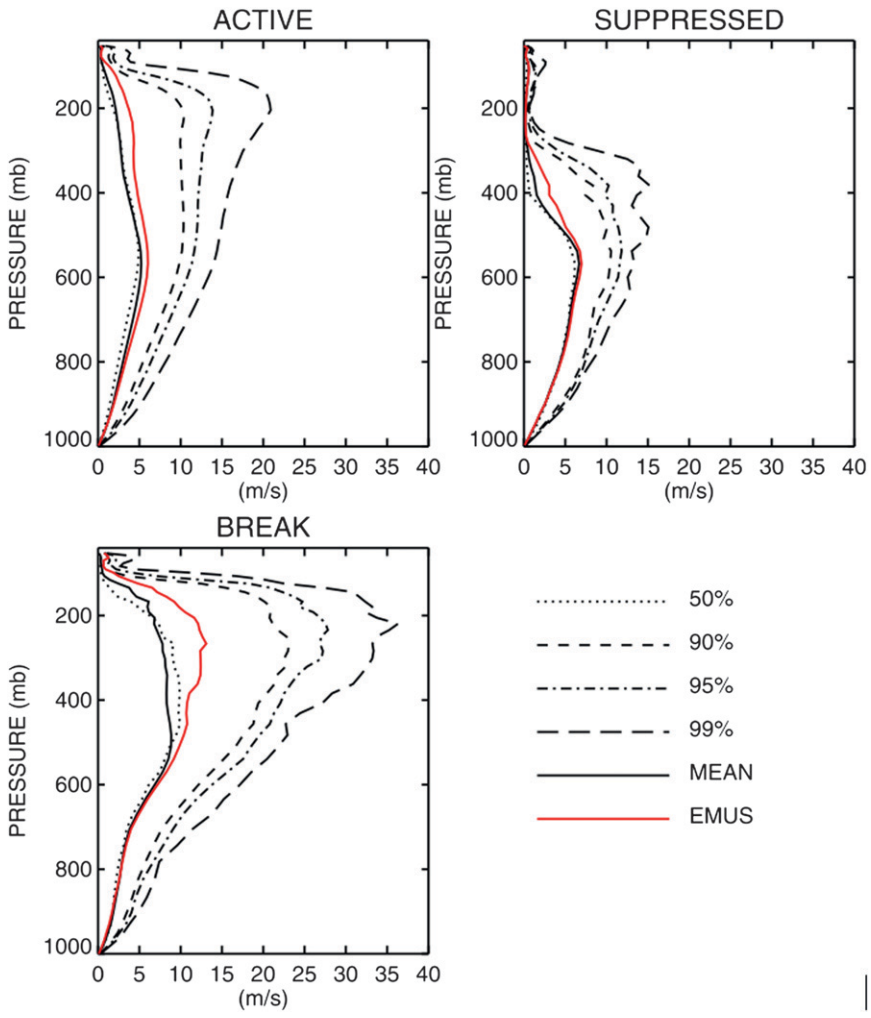

FIG. 13. Statistics of vertical velocities in convective cores [as reported in Wu et al. (2009), reproduced with permission]. The upper-left figure is for the same period of TWP-ICE used to derive Fig. 13 and shows significantly higher values. Please refer to the paper for details on the WRF modeling study and derivation of the figure.

Mean motions for the nonconditional dataset are very small as a result of upward motions being matched mainly by downward motions. While the fidelity of the multi-Doppler technique has not been discussed in detail here, it is safe to assume that it is not sensitive enough to measure domain mean motions because updrafts occupy only a small fraction of the domain. Of greater interest are the conditionally sampled data, as they give insight into the stronger vertical motions. The 99th-percentile DCC updraft reaches a maximum velocity of $8\,m\,s^{-1}$ at 400 hPa (~10 km). This is very different from the results from the WRF model (using Thompson-50 microphysics) reported in Fig. 3 from Wu et al. (2009) and reproduced in Fig. 13, which shows the 99th-percentile DCC only decelerating at the tropopause and peaking at $20\,m\,s^{-1}$. There are many possible explanations for this apparent overestimate of vertical velocity by the model, including lack of entrainment leading to highly nondiluted parcels, which undergo massive autoconversion to graupel releasing latent heat; however, in the absence of an in-depth study looking at other geophysical parameters this is merely speculation and is left to future study. While work remains to be done to better quantify the accuracy of the variational multi-Doppler technique (such as using the new multi-scale remote sensing facility at the ARM Southern Great Plains site in Oklahoma, where the profiling systems were, by design, located in the "sweet spot" for retrievals), results presented in section 3 show that the differences between model and observations are much larger than between the two estimates obtained from the dual-frequency profiler and from the scanning Doppler weather radars, giving

confidence that the profiles shown in Fig. 12 are reasonably representative for this period of TWP-ICE.

5. Conclusions

This paper has presented comparisons between variational retrievals of vertical velocity from volumetric scanning Doppler radars and a multifrequency profiler retrieval in the column. While the profiler retrievals are more direct vertical velocity estimates, the profiler cannot fully capture the three-dimensional structure of the storm. The overall motivation of this study is to assess the potential of scanning Doppler radar-derived vertical air motions for the statistical characterization of vertical air motions within convective storms on the mesoscale. To this end, we have compared the retrieved winds for three distinct cases during TWP-ICE. Despite issues in performing a one-to-one comparison with the profiler estimates, the updraft and downdraft structures compare very well between the two estimates (RMSE of $1.9\,\mathrm{m\,s^{-1}}$ and bias of $2.2\,\mathrm{m\,s^{-1}}$), suggesting that accurate updraft and downdraft statistics can be derived from scanning Doppler weather radar. Encouraged by these results, we performed retrievals for several days of radar data, from 0400 UTC 19 January to 2350 UTC 22 January 2006, a period roughly corresponding to the Global Energy and Water Cycle Experiment (GEWEX) Cloud System Study period. The 99th-percentile vertical velocity profile had a velocity maximum of $8\,\mathrm{m\,s^{-1}}$ at 400 hPa after convective cores were isolated and updraft statistics were computed. This velocity profile has a smaller peak magnitude occurring at a lower height than deep convective column 99th-percentile profiles presented in Wu et al. (2009). Future work will focus on building a longer record by looking at data outside the TWP-ICE IOP and investigating intraseasonal and season-to-season variability. In addition, a study is under way at the ARM Southern Great Plains site into the sensitivity of the retrieved vertical motions to various assumptions made in the technique.

Acknowledgments. Argonne National Laboratory's work was supported by the U.S. Department of Energy, Office of Science, Office of Biological and Environmental Research, under Contract DE-AC02-06CH11357. This work has been supported by the Office of Biological and Environmental Research (OBER) of the U.S. Department of Energy (DOE) as part of the ARM Program. Author CRW was supported by DOE Atmospheric Sciences Research (ASR) program Grant DE-SC0007080. We thank all involved in the TWP-ICE field program for their work in collecting a world-class dataset. Special thanks are given to Brad Atkinson and Dennis Klau for the continual upkeep of the CPOL radar. Thanks are also given to Kao-Shen Chung and Isztar Zawadzki for providing the original McGill multi-Doppler code. The bulk of the code has been written using the open-source NumPy and SciPy projects, and the authors are grateful to the authors of these projects. This manuscript has benefited greatly from reviews from Susan Rennie and Edwin Campos and the two anonymous reviewers.

REFERENCES

Ackerman, T. P., and G. M. Stokes, 2003: The Atmospheric Radiation Measurement Program. *Phys. Today,* **56,** 38–44.

Balsley, B. B., and K. S. Gage, 1982: On the use of radars for operational wind profiling. *Bull. Amer. Meteor. Soc.,* **63,** 1009–1018.

Carter, D. A., K. S. Gage, W. L. Ecklund, W. M. Angevine, P. E. Johnston, A. C. Riddle, J. Wilson, and C. R. Williams, 1995: Developments in UHF lower tropospheric wind profiling at NOAA's Aeronomy Laboratory. *Radio Sci.,* **30,** 977–1001.

Caya, A., 2001: Assimilation of radar observations into a cloud resolving model. Ph.D. thesis, McGill University, 31 pp.

Cifelli, R., and S. A. Rutledge, 1994: Vertical motion structure in maritime continent mesoscale convective systems: Results from a 50-MHz profiler. *J. Atmos. Sci.,* **51,** 2631–2652.

Collis, S., A. Protat, and K.-S. Chung, 2010: The effect of radial velocity gridding artifacts on variationally retrieved vertical velocities. *J. Atmos. Oceanic Technol.,* **27,** 1239–1246.

Fridlind, A. M., and Coauthors, 2012: A comparison of TWP-ICE observational data with cloud-resolving model results. *J. Geophys. Res.,* **117,** D05204, doi:10.1029/2011JD016595.

Fukao, S., K. Wakasugi, T. Sato, T. Tsuda, I. Kimura, N. Takeuchi, M. Matsuo, and S. Kato, 1985: Simultaneous observation of precipitating atmosphere by VHF band and C/Ku band radars. *Radio Sci.,* **20,** 622–630.

Gage, K. S., J. R. Mcafee, W. L. Ecklund, D. A. Carter, C. R. Williams, P. E. Johnston, and A. C. Riddle, 1994: The Christmas Island wind profiler: A prototype VHF wind-profiling radar for the tropics. *J. Atmos. Oceanic Technol.,* **11,** 22–31.

Gamache, J. F., F. D. Marks, and F. Roux, 1995: Comparison of three airborne Doppler sampling techniques with airborne in situ wind observations in Hurricane Gustav (1990). *J. Atmos. Oceanic Technol.,* **12,** 171–181.

James, C. N., and R. A. Houze, 2001: A real-time four-dimensional Doppler dealiasing scheme. *J. Atmos. Oceanic Technol.,* **18,** 1674–1683.

Keenan, T., K. Glasson, F. Cummings, T. S. Bird, J. Keeler, and J. Lutz, 1998: The BMRC/NCAR C-band polarimetric (C-POL) radar system. *J. Atmos. Oceanic Technol.,* **15,** 871–886.

May, P. T., 1999: Thermodynamic and vertical velocity structure of two gust fronts observed with a wind profiler/RASS during MCTEX. *Mon. Wea. Rev.,* **127,** 1796–1807.

——, and D. K. Rajopadhyaya, 1996: Wind profiler observations of vertical motion and precipitation microphysics of a tropical squall line. *Mon. Wea. Rev.,* **124,** 621–633; Corrigendum, **125,** 410–413.

——, and ——, 1999: Vertical velocity characteristics of deep convection over Darwin, Australia. *Mon. Wea. Rev.,* **127,** 1056–1071.

——, and T. P. Lane, 2009: A method for using weather radar data to test cloud resolving models. *Meteor. Appl.,* **16,** 425–425.

——, A. R. Jameson, T. D. Keenan, P. E. Johnston, and C. Lucas, 2002: Combined wind profiler/polarimetric radar studies of the vertical motion and microphysical characteristics of tropical sea-breeze thunderstorms. *Mon. Wea. Rev.,* **130,** 2228–2239.

——, J. H. Mather, G. Vaughan, K. N. Bower, C. Jakob, G. M. McFarquhar, and G. G. Mace, 2008: The Tropical Warm Pool International Cloud Experiment. *Bull. Amer. Meteor. Soc.,* **89,** 629–645.

Protat, A., and I. Zawadzki, 1999: A variational method for real-time retrieval of three-dimensional wind field from multiple-Doppler bistatic radar network data. *J. Atmos. Oceanic Technol.,* **16,** 432–449.

——, and ——, 2000: Optimization of dynamic retrievals from a multiple-Doppler radar network. *J. Atmos. Oceanic Technol.,* **17,** 753–760.

——, and C. R. Williams, 2011: The accuracy of radar estimates of ice terminal fall speed from vertically pointing Doppler radar measurements. *J. Appl. Meteor. Climatol.,* **50,** 2120–2138.

Ray, P. S., C. L. Ziegler, W. Bumgarner, and R. J. Serafin, 1980: Single- and multiple-Doppler radar observations of tornadic storms. *Mon. Wea. Rev.,* **108,** 1607–1625.

Reasor, P. D., M. D. Eastin, and J. F. Gamache, 2009: Rapidly intensifying Hurricane Guillermo (1997). Part I: Low-wavenumber structure and evolution. *Mon. Wea. Rev.,* **137,** 603–631.

Scialom, G., and Y. Lemaître, 1990: A new analysis for the retrieval of three-dimensional mesoscale wind fields from multiple Doppler radar. *J. Atmos. Oceanic Technol.,* **7,** 640–665.

Varble, A., and Coauthors, 2011: Evaluation of cloud-resolving model intercomparison simulations using TWP-ICE observations: Precipitation and cloud structure. *J. Geophys. Res.,* **116,** D12206, doi:10.1029/2010JD015180.

Wakasugi, K., A. Mizutani, M. Matsuo, S. Fukao, and S. Kato, 1986: A direct method for deriving drop-size distribution and vertical air velocities from VHF Doppler radar spectra. *J. Atmos. Oceanic Technol.,* **3,** 623–629.

Wang, W., and X. Liu, 2009: Evaluating deep updraft formulation in NCAR CAM3 with high-resolution WRF simulations during ARM TWP-ICE. *Geophys. Res. Lett.,* **36,** L04701, doi:10.1029/2008GL036692.

Williams, C. R., 2012: Vertical air motion retrieved from dual-frequency profiler observations. *J. Atmos. Oceanic Technol.,* **29,** 1471–1480.

Wu, J., A. D. D. Genio, M.-S. Yao, and A. B. Wolf, 2009: WRF and GISS SCM simulations of convective updraft properties during TWP-ICE. *J. Geophys. Res.,* **114,** D04206, doi:10.1029/2008JD010851.

Yuter, S. E., and R. A. Houze, 1995a: Three-dimensional kinematic and microphysical evolution of Florida cumulonimbus. Part I: Spatial distribution of updrafts, downdrafts, and precipitation. *Mon. Wea. Rev.,* **123,** 1921–1940.

——, and ——, 1995b: Three-dimensional kinematic and microphysical evolution of Florida cumulonimbus. Part II: Frequency distributions of vertical velocity, reflectivity, and differential reflectivity. *Mon. Wea. Rev.,* **123,** 1941–1963.